Carbon 184 (2021) 82–90

Contents lists available at ScienceDirect

Carbon

journal homepage: www.elsevier.com/locate/carbon

Research Article

Thermal stability studies of plasma deposited hydrogenated carbon nitride nanostructures

Eva Kovacevic [a, *], Thomas Strunskus [b], Neelakandan M. Santhosh [c, d], Janez Zavašnik [c, d], Wolfgang E.S. Unger [e], Thierry Sauvage [f], Mohamed-Ramzi Ammar [g], Uroš Cvelbar [c, d], Johannes Berndt [a]

[a] GREMI: Groupe de Recherches sur l'Energétique des Milieux Ionisés, UMR 7344, CNRS/Univeristé d'Orleans, 45067, Orléans Cedex 2, France
[b] Christian-Albrechts-University of Kiel, Institute of Material Science, 24143, Kiel, Germany
[c] Jožef Stefan Institute, Jamova cesta 39, SI-1000, Ljubljana, EU, Slovenia
[d] Jožef Stefan International Postgraduate School, Jamova cesta 39, SI-1000, Ljubljana, EU, Slovenia
[e] BAM -Federal Institute for Material Research and Testing, 12220, Berlin, Germany
[f] CEMHTI - Conditions Extrêmes et Matériaux: Haute Température et Irradiation - UPR3079, 45100, Orléans, France
[g] ICMN UMR7374, CNRS & Université d'Orléans, 45071, Orléans Cedex 2, EU, France

ARTICLE INFO

Article history:
Received 1 May 2021
Received in revised form
1 August 2021
Accepted 5 August 2021
Available online 6 August 2021

Keywords:
Carbon nanoparticles
Hydrogenated nanostructures
Plasma deposition
NEXAFS
Thermal annealing

ABSTRACT

Thermally stable carbon nitride nanostructures have potential applications in surface coatings and automotive fields. In this work, hydrogenated nitrogen-rich carbon nitride nanoparticles have been synthesised via low-pressure low-power plasma vapour deposition technique from methane/nitrogen gas mixture in a dry process. Thermal stability of the initially prepared hydrogenated carbon nitride structures has been analysed by near-edge X-ray absorption fine-structure spectroscopy (NEXAFS, *in-situ*), Raman spectroscopy, scanning and transmission electron microscopy and nuclear reaction analysis (NRA). Thermal studies reveal the excellent stability of the material and nitrogen-rich characteristics (N/C ratio 0.5–0.2 ± 0.01). The obtained results suggest transformation of sp^3-rich as-deposited carbon nitride into sp^2-carbon phase with more graphitic features upon thermal annealing. Such *in-situ* thermal studies of plasma deposited carbon nitrides confirm the conversion of sp^3-rich phase to sp^2-rich carbon phase at the critical temperature (about 450 K), without a huge loss in nitrogen content. The analysis revealed that the material is a stable plasma deposit after this critical temperature up to >1100 K. Additionally, super hydrophilic carbon nitride nanostructure transforms into a hydrophobic surface after thermal annealing. These thermally stable hydrophobic carbon nitride nanoparticles could be used as a promising material for the hydrophobic coatings for various applications, especially for harsh conditions.

1. Introduction

There have been extensive efforts taken to fabricate nitrogen incorporated/doped carbonaceous materials due to the ability of nitrogen to tailor the electrical, optical, and mechanical properties of the carbon materials. There are various nitrogen-containing carbonaceous forms reported so far, including nitrogen incorporated carbon nanotubes (CNT), graphene, graphene nanowalls, carbon nanofibers (CNF), nanoparticles, tholines and carbon dots. Apart from this, considerable research is taken to synthesise carbon nitride structures, which have higher bulk modulus and hardness than diamond [1,2]. Super hard properties and excellent tribological properties make them a potential candidate for automotive, optoelectronics, aerospace and surface coatings [3]. Several approaches have been practised to synthesise carbon nitride structures: sputtering, cathodic arc deposition, pulsed laser deposition, thermal annealing, and plasma-assisted deposition [1–11]. Crystalline form or graphitic carbon nitrides are produced in the processes like for example thermal evaporation or calcination [5–7]. Amorphous carbon nitride structures are formed in most cases when plasmas are used, and attempts have been made to transform them into crystalline phases by post-deposition thermal processing [8,9]. Although extensive studies on the synthesis of carbon nitrides are available, the obtained concentration of nitrogen in the carbon-

* Corresponding author.
E-mail address: eva.kovacevic@univ-orleans.fr (E. Kovacevic).

https://doi.org/10.1016/j.carbon.2021.08.008

nitrogen compounds are below the ideal composition for carbon nitrides [10]. The major difficulties in the synthesis of carbon nitrides are the disordered structure of the resulting material, its low thermodynamic stability, and the need for high temperature during the synthesis. To overcome these issues, several groups have tried to deposit carbon nitrides from the vapour phase by physical and chemical vapour deposition methods, yielding mostly amorphous products with a low concentration of nitrogen. Apart from these techniques, carbon nitride was successfully deposited by different plasma-enhanced chemical vapour depositions (PECVD) [4,11].

It has been widely known that plasma-assisted techniques could be useful for the large scale growth of 1D, 2D and 3D carbon nanostructures [12–14]. Additionally, plasma surface treatment has been used to incorporate foreign atoms into carbonaceous materials for tailoring the properties, mainly with nitrogen [15]. In this perspective, *in-situ* incorporation of nitrogen during the plasma-enhanced growth could be used as a promising method for the fast and easy controlled synthesis of carbon-nitride nanostructures on various substrates at relatively low-temperature. Like the other synthesis routes, the bottleneck of the plasma produced carbon nitrides is the thermal stability of the resulting materials. Thermal stability is of fundamental importance because it will determine the temperature range in which carbon nitrides can be used as surface coatings, for example, in the automotive and aerospace industries. It has been already found that thermal annealing can stabilise plasma deposited nanostructures and polymer composites by recombining trapped free radicals [11]. Post-deposition thermal treatments also promote the structural changes of amorphous to crystalline carbon nitrides by forming C–N bonds [9,16]. Thus, non-destructive characterisation techniques such as Raman and infrared spectroscopy can be useful for determining the bonding in carbon nitrides. Near edge X-ray absorption fine structure spectroscopy (NEXAFS) technique could be a potential *in-situ* tool to determine the changes that occur during the thermal annealing in a high vacuum. The structural changes and change in nitrogen concentration upon the thermal annealing can be assessed by the changes observed in the NEXAFS spectra of carbon and nitrogen. Furthermore, the internal stresses and defects of deposited material can be reduced by thermal annealing [17,18]. During the last decade, with increasing interest in carbon nitrides, many different annealing experiments concentrated on the compositional and structural changes of carbon nitride films [19–24]. Most stable carbon-nitride films presented in the literature do not decompose until about 1000 K, and other works reported the phase change from amorphous to crystalline. However, in most cases, the chemical composition analysis showed a significant loss of nitrogen (decrease of N/C ratio) during the annealing process [25].

Herein, we present *in-situ* thermal stability studies of the plasma deposited “carbon nitride” nanostructures using near-edge X-ray fine structure absorption spectroscopy (NEXAFS), accompanied by diverse ex-situ techniques. We call the material “carbon nitride” throughout the manuscript. However, we are aware that the starting material is a nitrogen-doped amorphous carbonaceous material that is transformed into a carbon-nitride-like material only upon annealing to high temperatures. Such nomenclature is established for this kind of plasma deposited material and refers to the material class “carbon nitrides” (usual for all CxNy compounds) rather than the crystalline stoichiometric C_3N_4 compounds known from the classical chemistry.

The carbon nitride nanoparticles (CNP) were synthesised by a low-temperature, low-pressure radio-frequency capacitively coupled plasma (RFCCP). This type of the synthesis of the nanoparticles, in the bulk of the plasma, between the electrodes, from a gas phase (in our case methane/nitrogen mixture) can be considered dry and green process. Such process can be used for deposition on any kind of surfaces, since the chamber and electrodes stay at room temperature. Low pressure systems allow us the control of the atmosphere around the substrates, and are very similar to widely spread technological processes (eg parallel plate PECVD systems), already used in industry. This method gives a possibility to deposit the films formed of nanoparticles with high porosity/effective surface area.

Morphology analysis of the carbon nitride particles indicated the formation of the spherical nanoparticles (analysed before and after thermal treatments by transmission electron microscopy - TEM). The annealing of the deposit and the changes occurring during the annealing were analysed systematically by means of NEXAFS. Raman spectroscopy was used to analyse the structural quality of the carbon nanostructures. Moreover, the elemental analysis of the material was performed before and after the annealing by Nuclear Reaction Analysis (NRA). The results indicate a decrease in the N/C ratio after annealing. Additionally, the investigation reveals material transformation from sp^3 phase to sp^2 rich phase upon thermal annealing.

2. Materials and methods

2.1. Synthesis of hydrogenated carbon nitrides

Synthesis of carbon nitride nanostructures was carried out in a radio-frequency capacitively coupled discharge driven by 13.56 MHz. The plasma system consists of two 13 cm electrodes. The upper electrode was the powered electrode. The lower electrode was the grounded electrode, and the electrodes were separated by a distance of 5 cm [26]. The nanostructures were deposited onto standard <111> silicon wafers, chemically treated Si wafers (where the native oxidised layer was removed using HF acid treatment and heating) and Ta wafers (thickness ~250 μm). The type of substrates is connected with technological applications and targets different characterisation methods, and the processing and analysis were performed on all of the substrates in the same manner for direct comparison. The plasma system was pumped down to 10^{-6} mbar before the experiments. A gas mixture of methane/nitrogen-containing 10 % methane at a flow rate of 50 sccm was fed as precursors for the deposition at a pressure of 1 mbar (different mixtures can give slight changes of the nitrogen content, non-existent nanoparticles or unstable plasmas; thus, this specific mixture is chosen as an example of optimum conditions). The nanoparticles were produced simply by switching the plasma on for the film/dust formation using an input power of 40 W. As described previously [11,27,29], the synthesis of the nanoparticles occurs in the gas phase, from ion clusters forming nuclei, which are under the size of few nanometres both positively and negatively and heated by the presence of ions and electrons. After reaching a certain critical size, the nuclei of about 10 nm in size remain levitating between the electrodes, negatively charged by the fastest species in the plasma electrons. These nuclei grow further by the ballistic deposition (impinging of positive ions and neutrals) until we stop the process, or until the particles get too large for the forces holding them between the electrodes. In our case, since the particles grow almost monodisperse, we chose the time when they reach about 80 nm (about 2 min) and switch off the discharge, which causes that the nanoparticles fall onto the substrates. Since there are no thermal processes and no external heating used during the synthesis and deposition, and in given low-pressure low-power CCP conditions, the effect of the plasma heating of the substrate is negligible during the discharge and all of the devices are hold on the room temperature (hence the name low-temperature or cold plasma). The substrate can be any material from plastics to metallic surfaces. Vice versa, the substrates do not have any influence on the

material deposition. The procedure was repeated for 1–10 cycles of growth for the deposition of thicker layers. With 3 growth cycles, we have covered surfaces relatively homogeneously, whereas 10 cycles give a spongy structure as e.g. in Ref. [23] (to, 1 cycle consist of few steps: plasma on, the onset of the nanoparticles, short growth, switching off when targeted size of nanoparticles is reached, nanoparticles falling onto the substrates, which we consider as deposition). The thickness for further measurements was chosen to obtain reliable NEXAFS, Raman and NRA measurements, and it does not change the effects of the treatment. The particle formation is monitored by the analysis of electrical characteristics of the discharge (e.g. self-bias) [11,27]. This observation of the plasma allows the *in-situ* identification of different growth phases related to specific particle sizes and, thus, controlled production of the particles described in detail elsewhere [25,28]. Briefly: the changes in these characteristics were related to the size of the nanoparticles by means of collection of the nanoparticles, and their ex-situ analysis by SEM and TEM, in order to make correlation between the nanoparticle size (the growth phase) and the self-bias or electrical characteristics. Thus it is easy to know the size of the nanoparticles and stop the growth process based on even the slightest changes in eg self bias, or reflected power.

2.2. Characterisation techniques

The samples before and after the annealing were analysed by transmission electron microscope (TEM, JEM-2100, Jeol) operating at 200 kV. The powdered samples were scratched from the template and directly deposited onto the amorphous lacey-carbon support grids without further treatment. Low-background beryllium double-tilt holder was used for analyses, while micrographs were recorded by a slow-scan CCD camera (Orius SC1000, Gatan). The surface morphology of the deposited film-like structure was characterised by scanning electron microscopy (SEM, Supra 40, Zeiss). Raman spectra of the samples were recorded using a Renishaw InVia Reflex Spectrometer at an excitation wavelength of 785 nm. The material as deposited on Si substrates was analysed first employing FTIR in transmission mode using a Bruker Equinox 75 spectrometer. The stoichiometry of the carbon nitrides was measured before and after the annealing by nuclear reaction analysis (NRA) using the 3 MV electrostatic accelerator at CEMHTI Orléans. The measurement of nitrogen, carbon and oxygen areal densities is performed by detection of light particles (protons or alphas) emitted from the ^{14}N $(d,p_5)^{15}N$, ^{12}C $(d,p_0)^{13}C$ and ^{16}O $(d,\alpha_0)^{14}N$ nuclear reactions, respectively. A 2×2 mm^2 primary deuteron beam impinges the sample at normal incidence with an energy of 950 keV. The emitted protons and alphas are detected with a 25 mm^2 detector located at an angle of 150° to the beam direction and a distance of 70 mm from the sample surface. The accumulated D^+ charge required to obtain good counting statistics of N, O and C signals is 10 μC. The beam current is reduced to a value of 3 nA to avoid material damages under irradiation. The experimental spectra were simulated using the SIMNRA program [50, 51] [7] M. Mayer, SIMNRA user's guide, *Report IPP* vol. 9/113, Max-Planck-Institut fur Plasmaphysik, Garching, Germany (1997)to determine the stoichiometry and the areal density of the different elements. The change in surface chemistry also influenced the wettability and static contact angle for water and was measured with DIGIDROP, GBX [26].

2.3. In-situ annealing and thermal stability measurements

Thermal stability of the prepared carbon nitride nanostructures was examined on the samples deposited onto the tantalum (Ta) substrates. The *in-situ* annealing experiments and thermal stability measurements were carried out in an ultra-high vacuum chamber of the end station at the HESGM beamline at BESSY II. The effect of the annealing on the nanostructures was investigated by means of near-edge X-ray absorption fine structure spectroscopy (NEXAFS). Measurements were performed at an incident angle of 55° (magic angle) relative to the substrate surface. Data were obtained on C, N and O K edge, in the total electron yield (TEY) mode (information depth in the range <10 nm [49], using a home-built double-channel plate detector. The energy resolution was ≈0.40 eV at the C K edge, ≈ 0.55 eV at the N K edge and ~ 0.6 eV at the O K edge. All spectra have been referenced against a peak at 284.9 eV in simultaneously recorded I_0 spectra of a carbon contaminated Au grid, which has been referenced previously against the π*-the resonance of highly oriented pyrolytic graphite at 285.4 eV. Each presented spectrum is an average of at least 4 sweeps. The raw NEXAFS spectra were normalised to the incident photon flux and corrected for the beamline transmission by division through a spectrum of a clean, freshly sputtered Au sample.

3. Results and discussion

The surface of all substrates was covered with hydrogenated carbon-nitride nanoparticles in the form of a thin-film is observed from SEM micrographs as shown in Fig. 1. a, similarly reported in previous studies [11,26,27]. IR measurements in transmission mode have been performed on the materials deposited onto cleaned Si wafers to identify the chemical compositions. Fig. 1b shows the ex-situ IR spectrum of the deposited nanostructures produced in a nitrogen/methane gas mixture. The broad, strong features with a maximum at about 3300 cm^{-1} can be identified as NH stretching vibrations (NH_2 and NH_3, overlapping with a certain small amount of OH stretching bonds due to impurities present in the chamber) [29]. The shoulder around 2930 cm^{-1} is identified as CH stretching feature (CH_2 and CH_3, symmetric and asymmetric). The dominant feature in the spectrum is a strong, broad absorption band centred at about 1625 cm^{-1}, which can be interpreted mostly by the formation of CN double bonds, with possible C=C presence as well as a superposition of vibrations with different origins (e.g. C=O, CH bending) [2]. The presence of triple bonds is observable from the feature showing a maximum at about 2200 cm^{-1}. The origin of this feature is C≡N (nitrile, isonitrile) [29,30]. These bands correspond to the bands reported for hydrogenated amorphous carbon-nitride (a-C: H–N) films or nanoparticles produced using low-pressure plasma polymerisation of hydrocarbons mixed with N_2 or NH_3 [2,11,30,31].

To gain a better understanding of different bonding configurations, the chemical analysis of the nanocomposites is carried out by performing NEXAFS measurements. NEXAFS is a very promising technique, suitable for resolving the different bonding situations in nanostructures and thin films with high sensitivity for unsaturated species. The NEXAFS spectra are acquired with the nanostructures deposited on Ta wafers because of the good thermal stability and thermal conductivity of Ta substrate at high temperatures. However, the same experiments with the same results were obtained from Si wafers, too. NEXAFS spectra of the as-deposited hydrogenated carbon nitride nanoparticles are presented in Fig. 1c and d. The NEXAFS spectra have been normalised to the adsorption edge in the C K-edge spectrum. The peak resonance is assigned corresponding to the resonances observed in the related literature [31,32].

The C K-edge spectra of the as-deposited hydrogenated carbon nitride structures (Fig. 1c) consist of a broad pre-edge shoulder C1 in the range 285–286 eV is ascribed to the superposition of at least two components, the one near 285 eV is a typical characteristic of transitions to π* orbitals related to phenyl rings and non-

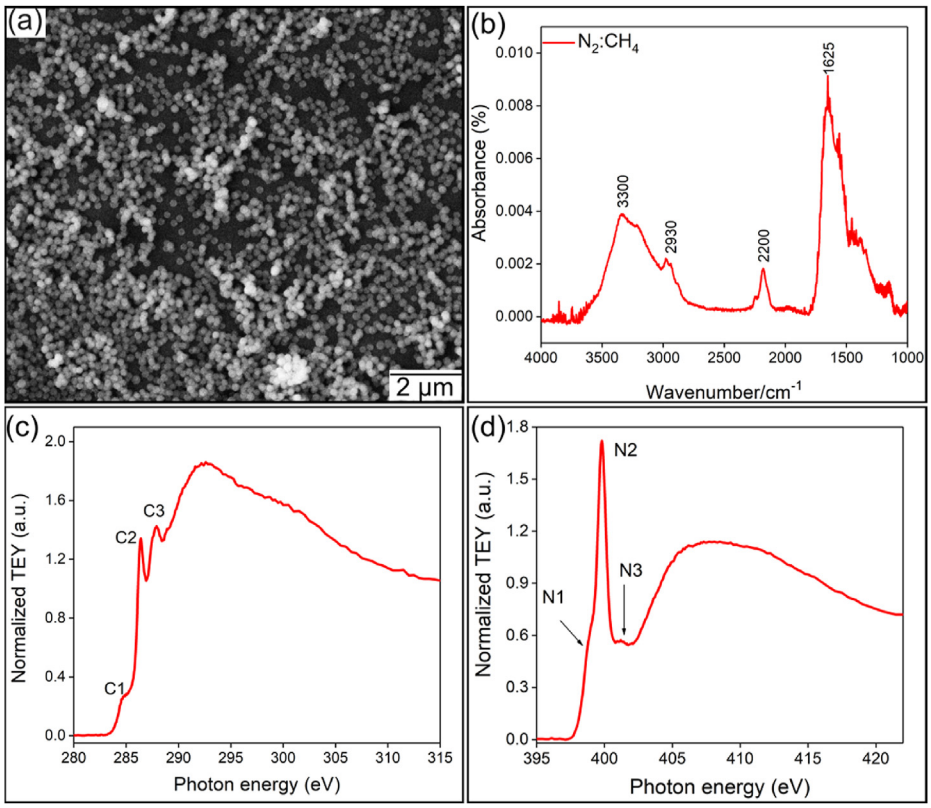

Fig. 1. Surface and structural characteristics of hydrogenated carbon nitride nanostructures as-deposited: (a) SEM secondary electrons (SE) micrograph of spherical hydrogenated carbon nitride nanoparticles; (b) ex-situ FTIR spectrum; (c) NEXAFS spectrum: C K-edge, d) NEXAFS spectrum: N K-edge. (A colour version of this figure can be viewed online.)

conjugated double bonds [33,34]. Furthermore, a π*(C═N) resonance is known to appear near 285.5 eV, which could also contribute to the pre-edge shoulder C1. These findings reveal that the amount of C═C bonds present at the surface is rather low. In addition to C1 peak, the C2 feature appeared at 286.4 eV and is assigned to C1s→π* (C≡N) resonance, similar to the resonances observed in nitrogen-containing conductive polymers [35,36]. Furthermore, the broad C K-edge feature C3 at around 288 eV can be assigned to the possible contribution from amide groups. An amide related π* resonance at 288.2 eV has been reported in the literature [35,36]. Nevertheless, C3 also exhibits a shoulder peak at about 287.7 eV suggesting contributions from other species or due to resonance splitting related to conjugation phenomena. This can be due to the plasma-assisted deposition, which could result in the formation of nanostructures with a large variety of bonding situations. The peak resonance observed above the absorption edge, around 292 eV can be ascribed to the different C1s→σ* resonances, in which the shape and position are typical for low-temperature plasma polymerised/deposited samples [11,37]. Moreover, there is a distinct feature around 301 eV, probably originating from σ* resonances of unsaturated carbon species [38].

Further investigation on the bonding situations of nitrogen in the hydrogenated carbon nitride nanostructures is analysed by the N K-edge spectra (Fig. 1d). The dominant resonances observed in the as-deposited hydrogenated carbon nitrides are N1 at ~398.9 eV and N2 at ~399.7 eV, representing the π* resonances from the unsaturated nitrogen bonds. Typically, N1 can be related to the constrained CN bonds, the presence of pyridine-like double bonds (-C═N-), or imines [15,39]. Similarly, conjugated C═C–C≡N moieties are reported to show a manifold of resonances with an intense component at this energy range [40]. N2 resonance at 399.7 eV is ascribed to the N≡C bonds (nitriles, isonitriles), similarly reported in the literature and these findings strongly correlate with the vibrations observed in the IR spectra (2200 cm^{-1}). The weak feature that appeared in the IR spectra can be due to the weak absorption of aliphatic nitriles; however, NEXAFS is very sensitive to the presence of these groups and shows a pronounced resonance at this region [11,36,41,42]. A weak resonance observed at 401 eV (N3) might be correlated to amines or nitrogen substituted carbons in aromatic systems [43–45]. However, in this study, the possibility of substituted nitrogen in the graphitic environment can be neglected concerning the C K-edge spectrum of the sample. Furthermore, we can observe a change of the slope around 402 eV and a strong, broad σ* resonance around 407 eV, which can be due to the transition of N 1s → σ *(N–H, N–C) [36]. The surface analysis of the as-deposited hydrogenated carbon nitrides shows significant similarities with the amorphous type carbon nitrides. Thus, post-deposition processing of the hydrogenated carbon nitrides was performed to observe the structure and chemical composition changes by *in-situ* thermal annealing during NEXAFS measurements.

The annealing experiments were performed in several steps, with a heating rate of about 20 K/min and holding the desired temperature for 10 min. The annealing was performed in the temperature range 300–1100 K, and the results are represented in which significant changes are observed. The NEXAFS spectra obtained during the annealing experiment are presented without normalisation to the absorption edge to check the possible changes of the material resulting in changes in the electron yield intensities. The only pre-treatment is as following: the pre-edge at 280 eV is normalised for all spectra to avoid effects of the measurement artefacts e.g. lower ring current and lower detector amplification.

Changes observed in the C K-edge spectra at different annealing temperatures are presented in Fig. 2a. Compared to the room temperature (300 K), the significant changes in the spectra observed at 600 K. It has been evident that the C1 intensity comprising π* (C═C, C═N) resonances is increasing, and a small gradual loss of C3, probably representing amides with the annealing. A further increase to 650 K resulted in the dominance of C═C and C≡N resonances over other bonds, in which C1 and C2 peaks dominate the pre-edge region. After 650 K, the peaks C2 and C3 are present only as a shoulder on the C1. From 700 K to 1100 K, the shape of the spectra remains rather stable. It is similar to the C K-edge observed in the thermally annealed tetrahedral amorphous carbon nitride films [46]. An increase in total electron yield (TEY) intensity of the spectra during the thermal annealing can be due to the increase in conductivity of the resulting material and higher electron gain, which is evident for the increase in the structural organisation of the amorphous carbon nitride films upon annealing.

Fig. 2b exhibits the N K-edge NEXAFS spectra at the similar annealing temperatures presented for C K-edge. The spectra are almost similar to the as-deposited hydrogenated carbon nitride structures until an annealing temperature of 650 K, where the N1/N2 area ratio is slightly varied. However, at 650 K, the spectra reveal a drastic spectral change, where the N1/N2 resonance area ratio changes in favour of N1, and N3 becomes pronounced (Fig. 2c). The origin of the N3 feature can be ascribed to the changes from amines present in the as-deposited or annealed samples (T < 650 K), to N atoms in graphitic surroundings [45]. Moreover, the pre-edge region becomes gradually weaker in intensity with the further increase of temperature, to 700 K–1030 K. The low intensity of the spectra from 800 K can be correlated with material loss and changes in density occurring at this temperature. Still, there are no further variations observed in spectral shape. As shown in Fig. 2c, nitrile groups are lost from the nanostructures at low temperatures, while pyridinic (N1) and graphitic bonds are stable up to 650 K.

The TEY intensities (integration limits 396 eV–435 eV) of the N K edge spectra vs annealing temperature are presented in Fig. 2d to understand the nitrogen configuration changes upon annealing. The development of the nitrogen content in the films during the annealing of the nanocomposite can be qualitatively derived from this graph. Changes are small for temperatures between 300 and 600 K. The N content is decreasing after 650 K and reaching a stable level above 850 K. However, additional precise elemental analysis, like nuclear resonance analysis (NRA), is necessary for a quantitative determination of the material constituents in terms of N/C ratios. A characteristic NRA spectrum of the as-deposited nanocomposite is presented in Fig. 2e, referring to all the measured reactions. For N/C determination, we used the N peak originating from the $^{14}N\,(d,p_5)^{15}N$ reaction [47] and the C peak originating from the $^{12}C\,(d,p_0)^{13}C$ reaction [48]. The first results on the elemental composition (C/N ratio) derived from SIMNRA simulation are 0.50 ± 0.02 for as-deposited samples. The NRA of the sample also confirms oxygen is a constituent of the sample at a concentration level of a few atomic percent. The feature at 286.4 eV likely also includes some minor contributions from carbonyl groups, usually found at this position [36].

Considering this fact and the presence of amides observed in the C K-edge, this can also be explained as the co-existence of the bonded oxygen. Thus, a detailed investigation on the O K-edge of the samples was conducted and the changes in the NEXAFS spectrum at similar annealing temperatures presented in Fig. 3a. Two principal resonance features at the O K-edge are observed: the pre-

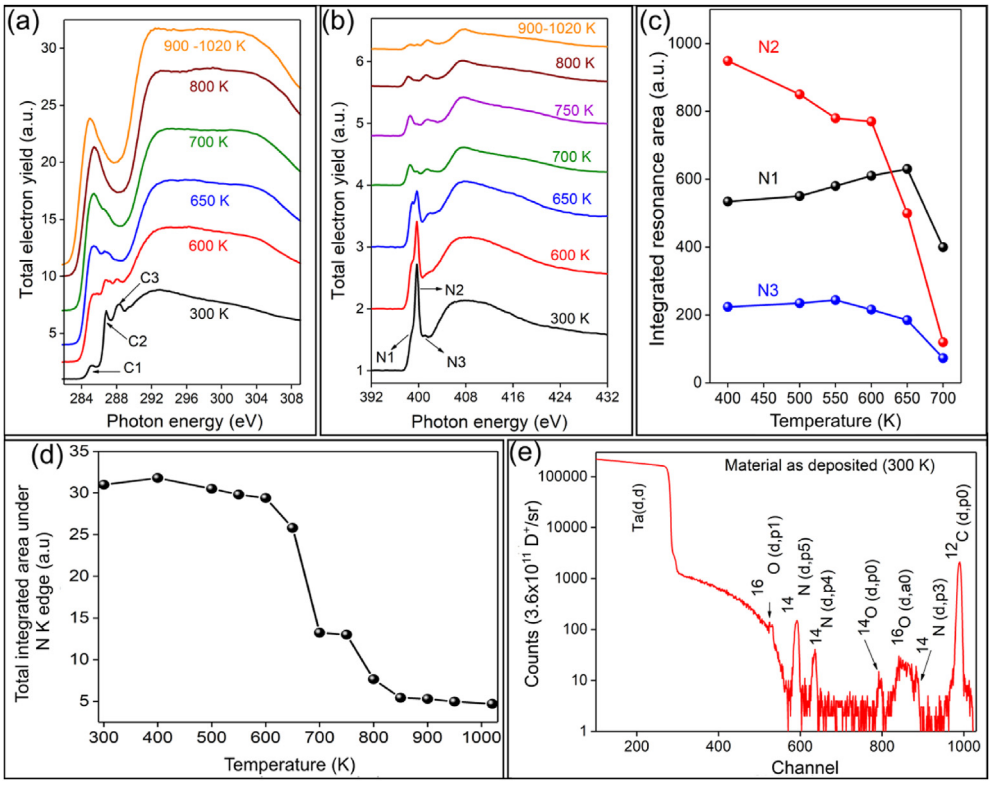

Fig. 2. Annealing of nanocomposite: (a) NEXAFS spectra at C K-edge, b) NEXAFS spectra at N K-edge, (c) NEXAFS N K-edge data: the behaviour of resonances at 398.7 eV (N1: constrained CN bonds, pyridine-like double bonds (–C═N–) or imines); 399.7 eV (N2: nitriles, unsaturated multiple CN bonds) and 401 eV (N3: amines and N in graphitic surroundings) during annealing of polymer; data represent the integrated resonant areas; (d) integral over the nitrogen K edge spectra at every temperature step (integration limits 396–435.5 eV); (e) NRA spectrum of nanocomposite: identification of spectral features (nuclear reactions). (A colour version of this figure can be viewed online.)

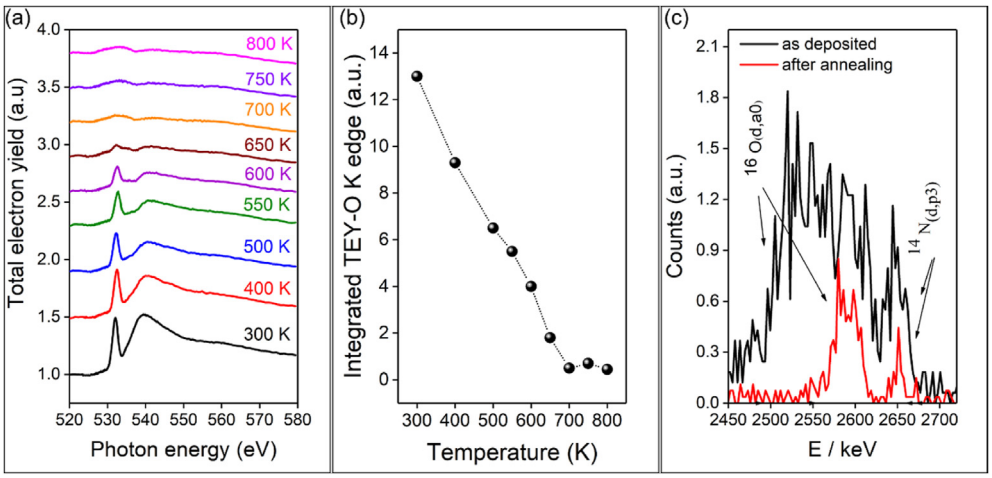

Fig. 3. Oxygen behaviour: (a) NEXAFS spectra at O K-edge during annealing of hydrogenated carbon nitride; (b) integral over the oxygen K-edge spectra (integration limits 524–570 eV) at every temperature step during annealing process; (c) oxygen peak originating from ^{16}O (d, alpha)^{14}N reaction (details from NRA spectra of CN nanocomposite) of as-deposited material and after annealing at 1100 K. (A colour version of this figure can be viewed online.)

edge carbonyl π* resonance at 533 eV, and σ* resonances above ~537 eV with a maximum at 539 eV. The first one is correlated with 1s →π* (O═C), as well as conjugated carbonyls. The pre-edge π* resonance at 533 eV (correlated with 1s →π* (O═C), as well as conjugated carbonyls), and σ* resonances above ~ 537 eV with a maximum at 539 eV. The intensity of the whole spectrum is decreasing with increasing temperature. Moreover, there are subtle changes in the intensity ratios of π* and σ* resonances (at O K edge) during annealing. It is seen that σ bonds are decreasing more rapidly, opposite to the behaviour observed at O K edge by annealing of nitrogen-containing carbon nanotubes [49]. The loss of oxygen from the sample upon the annealing derived from integrated areas under O K-edge NEXAFS is illustrated in Fig. 3 (b) (integration limits 524–570 eV). Fig. 3b indicates that the decay of oxygen bonds starts already at rather low temperatures of 400 K, and the oxygen content is negligible for temperatures above 650 K. The complete loss of oxygen already at 650 K indicates that oxygen is not contained in the main C–N network, but only present inside groups. The question rises about the reoxydization of the annealed nanocomposite after removal from vacuum and exposure to air. This can be answered again with NRA results (both metallic and intrinsic Si wafer as substrates), from the peak of alphas around 2450–2600 keV originating from ^{16}O (d,α_0)^{14}N reactions, that provides the information on the oxygen depth profile [50]. The data at higher energies are correlated with reactions on the surfaces, and the data for smaller energies correspond to the reactions that occur deeper in bulk.

Comparison of this NRA feature of the carbon nitride nanostructures as deposited to one that annealed and long-term exposure is presented in Fig. 3c, where the spectra are normalised to tantalum Rutherford backscattering plateau. In the case of the as-deposited material, the peak is broad, from 2480 to 2620 keV. In the annealed material, the peak is lower and rather narrow (FWHM ~30 keV). In both cases, the weak peak of ^{14}N (d,p_3) reaction is observable at 2666 keV but not interfere with ^{16}O (d,α_0)^{14}N signal used for O depth profile determination.

The difference observed in Fig. 3c suggests that the oxygen for the annealed material is concentrated at and near the deposit surface due to the long-time exposure of the annealed material to the atmosphere. The presence of oxygen in the as–deposited material is in the range of a few percent; hence after annealing, according to NRA results, it can be neglected. Additionally, the NRA results give additional insight into the N and C composition, showing the N/C ratio decrease from 0.50 (±0.02) to 0.20 (±0.02) after annealing at 1020 K. Concerning this change of the N/C ratio after the annealing, it has been evident that there is a nitrogen loss accompanied by a minor material loss. This result confirms the NEXAFS data, since NRA measurements provide information on elemental abundances throughout the bulk. Thus, a further investigation is carried out for identifying the morphological and structural changes that occurred after the thermal annealing.

The surface morphology of the as-deposited hydrogenated carbon nitride nanostructures is similar to the morphology reported in previous experiments [11]. The samples before and after annealing were investigated by TEM and the results are presented on Fig. 4. There are no significant differences in spatial distribution and agglomeration of the particulates before and after annealing, as seen on overview TEM micrographs on Fig. 4a,a'. The initial, as-synthesised sample before the annealing consists of spherical particles with size of 60–90 nm (Fig. 4b,e). The carboniferous spheres are highly amorphous and are firmly intergrown with a large contact area between the spheres (Fig. 4b,d). The surface of the spheres appears smooth (Fig. 4c), while after the annealing, the sphere-like particles appear rougher, with a more pronounced morphology, as seen in Fig. 4b'. The close-up of the sample surface reveals numerous carbon fibrils loosely intertwined (Fig. 4c'). After annealing, the size of the spheres is slightly decreased, with the majority of the particulates in size of 50–80 nm (Fig. 4e'). The crystallinity of the samples before and after the annealing was probed by TEM-based selected area electron diffraction (SAED). The original sample is highly amorphous, while after the annealing we can observe an increased electron scattering at crystal planes separated for 2.15 and 1.20 A, which correspond to {004} (c-axis) and {110} (a, b-axis) crystal planes (Fig. 4d).

Carbon nitride samples were analysed by Raman spectroscopy to investigate the changes in their structural organisations upon annealing (Fig. 5a). Several unsuccessful attempts, due to fluorescence, have been made to record the Raman spectrum of as-deposited carbon nitride using several excitation energies in the visible range. The annealing process resulted in the appearance of well-distinguished characteristic peaks of sp^2-rich phases of carbon located at 1359 cm^{-1} and 1589 cm^{-1} corresponding to D and G bands. This is mainly due to the thermal conversion of sp^3 to sp^2 phases (metastable-stable transformation). The material loss

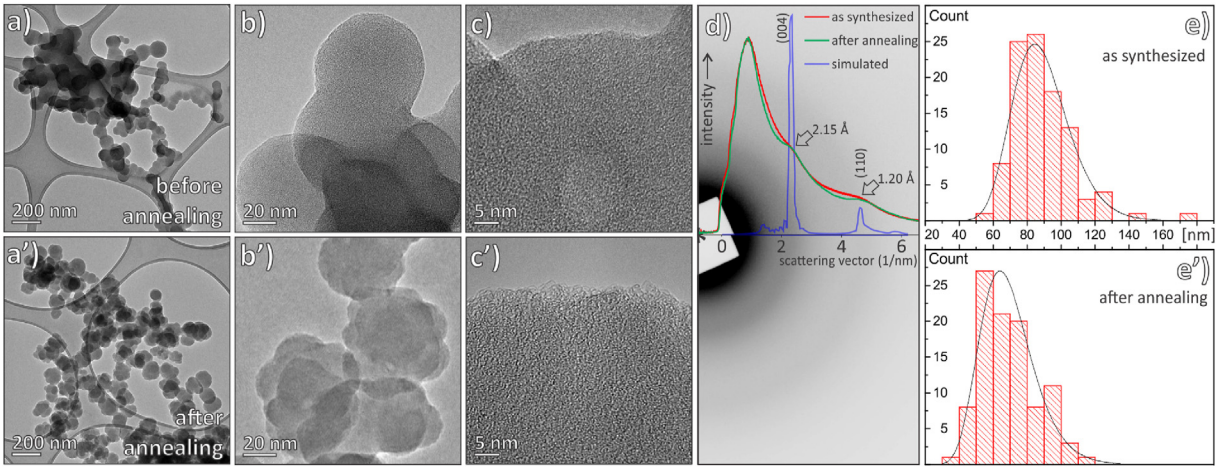

Fig. 4. TEM micrographs of the samples before (top row) and after annealing (bottom row); (a, a') overview low-magnification TEM micrographs of spherical particles and their spatial arrangement. (b, b') The morphology differences before and after the annealing, showing smooth and structured morphology. (c, c') The surface of the spheres transitions from smooth to loose intertwined carbon fibres. d) SAED diffraction patterns (top-half: original, bottom-half: annealed samples) and corresponding intensity graphs of as synthesised (green) and annealed (red) sample, with simulation for graphite (blue). After annealing, the peaks at 2.15 Å and 1.20 Å are marked with arrows, and coincides with {004} and {110} planes of graphite. (e, e') Particle size distribution histogram before and after the annealing, N = 100. (A colour version of this figure can be viewed online.)

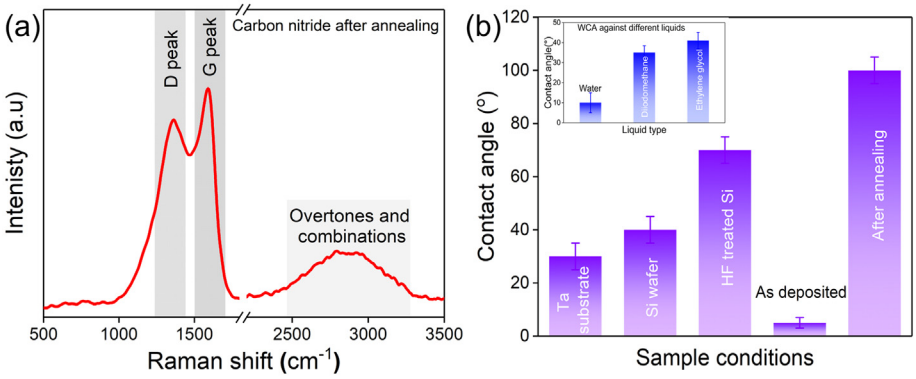

Fig. 5. (a) Raman spectra of thermally annealed hydrogenated carbon nitride nanoparticles; (b) water contact angle (WCA) measurements of the carbon nitride nanoparticle film and the wettability towards different liquid types (inset) (important to stress that the angle was same for the deposits on all types of substrates, and that original angles are about 30° for Ta, ~70° for HF cleaned Si, and ~40° for standard monocrystalline 111 Si wafer). (A colour version of this figure can be viewed online.)

during the annealing can be ascribed to the loss of heterogeneous atoms from the sample.

These findings indicate that the surface chemistry of the carbon nitride structures was changed during the thermal treatment and the wetting property of the samples towards the water was analysed by measuring the static water contact angle and presented in Fig. 5b). The as-deposited samples show a contact angle of below 5°, corresponding to the super hydrophilic property of the hydrogenated carbon nitride nanostructures (this also explains the way nanoparticles stick to each other, forming a spongy structure). On the other hand, thermally annealed samples show a large deviation from the initial value to 100 ± 5°, indicating that the surface property is changed towards a hydrophobic surface, which can be due to the loss of hydrogen and oxygen upon annealing (important to stress: intrinsic WCA for clean Ta substrate was about 30°, HF cleaned Si wafer 70° and intrinsic <111> Si wafer about 40°). Consequently, *in-situ* thermal annealing studies reveal that the amorphous sp^3-rich phase of hydrogenated carbon nitrides transforms to sp^2 rich phase upon thermal annealing. The nitrogen groups in the material are stable up to 650 K, and a visible loss is observed after 700 K. The thermal annealing causes the change in the surface chemistry from hydrophilic to hydrophobic.

4. Conclusions

Herein, we have synthesised hydrogenated carbon nitride nanostructure and studied the thermal stability of the material. The spherical carbon nitride nanostructures are synthesised using a low-pressure plasma system. As-deposited hydrogenated carbon nitrides are enriched with an sp^3-rich phase. *In-situ* thermal studies and ex-situ material analysis reveal the excellent stability of the material under critical temperature and transformation of the sp^3 rich phase to sp^2 rich phase upon thermal annealing (again, the material stays stable after critical temperature). Additionally, super hydrophilic properties of as-deposited hydrogenated carbon nitride nanostructure changed to a hydrophobic surface after the thermal annealing. Such *in-situ* thermal studies of plasma deposited hydrogenated carbon nitrides confirm the increase in the structural organisation, stability and change in surface properties of the plasma deposited carbon nitrides, which could be used as a promising material for the hydrophobic coatings for various applications. One more piece of information important for applications is that the ageing tests on the first produced samples were done over 10 years, showing none of the properties of the material ageing during this long period.

CRediT authorship contribution statement

Eva Kovacevic: Conceptualisation, Methodology, Formal analysis, Data curation, Writing, reviewing and editing the draft, Validation, and, Funding acquisition. **Thomas Strunskus:** Data curation, reviewing and editing the draft. **Neelakandan M. Santhosh:** Data curation, Methodology, Writing and editing the draft. **Janez Zavašnik:** TEM analyses, Data curation, Writing – review & editing, the manuscript. **Thierry Sauvage:** Data curation, reviewing and editing the draft. **Mohamed-Ramzi Ammar:** Data curation, reviewing and editing the draft. **Uroš Cvelbar:** Reviewing and editing the draft. **Johannes Berndt:** Reviewing and editing the draft, Validation and Funding acquisition.

Declaration of competing interest

The authors declare that they have no known competing financial interests or personal relationships that could have appeared to influence the work reported in this paper.

Acknowledgements

Authors acknowledge the support of PEGASUS (Plasma Enabled and Graphene Allowed Synthesis of Unique Nano-structures) project, funded by the European Union's Horizon research and innovation program under grant agreement No. 766894. Experiments at BESSY have also been supported with H2020 Calypso Plus project, grant Nr. 19208955-ST and 19108281-ST/R., 192-08646-ST, and 18106986 -ST. as well as by BMBF 05 ES3XBA/5 and EC under IA-SFS Contract RII3-CT2004-506008. Authors would like to thank the personnel at BESSY II, for support during our activities at the HE-SGM beamline; as well as Dr. A. Nefedov for providing helpful discussions.

References

[1] A.Y. Liu, M.L. Cohen, Prediction of new low compressibility solids, Science (80-.) (1989), https://doi.org/10.1126/science.245.4920.841.
[2] A.C. Ferrari, S.E. Rodil, J. Robertson, S.E. Rodil, J. Robertson, Interpretation of infrared and Raman spectra of amorphous carbon nitrides, Phys. Rev. B Condens. Matter (2003), https://doi.org/10.1103/PhysRevB.67.155306.
[3] E.G. Wang, Research on carbon nitrides, Prog. Mater. Sci. (1997), https://doi.org/10.1016/s0079-6425(97)00027-3.
[4] S. Kobayashi, S. Nozaki, H. Morisaki, S. Masaki, Hydrogenated carbon nitride thin films deposited by the plasma chemical vapor deposition technique using trimethylamine and ammonia, Jpn. J. Appl. Phys. 36 (1997) 5187–5191, https://doi.org/10.1143/JJAP.36.5187.
[5] Z. Liu, C. Wang, Z. Zhu, Q. Lou, C. Shen, Y. Chen, J. Sun, Y. Ye, J. Zang, L. Dong, C.X. Shan, Wafer-scale growth of two-dimensional graphitic carbon nitride films, Matter 4 (2021) 1625–1638, https://doi.org/10.1016/j.matt.2021.02.014.
[6] Q. Cao, B. Kumru, M. Antonietti, B.V.K.J. Schmidt, Grafting polymers onto carbon nitride via visible-light-induced photofunctionalization, Macromolecules 52 (2019) 4989–4996, https://doi.org/10.1021/acs.macromol.9b00894.
[7] J. Qin, J. Barrio, G. Peng, J. Tzadikov, L. Abisdris, M. Volokh, M. Shalom, Direct growth of uniform carbon nitride layers with extended optical absorption towards efficient water-splitting photoanodes, Nat. Commun. 11 (2020) 1–9, https://doi.org/10.1038/s41467-020-18535-0.
[8] L. Hultman, Thermal stability of nitride thin films, Vacuum (2000), https://doi.org/10.1016/s0042-207x(00)00143-3.
[9] G.L. Chen, Y. Li, J. Lin, C.H.A. Huan, Y.P. Guo, Crystallization by post-treatment of reactive r.f.-magnetron-sputtered carbon nitride films, Diam. Relat. Mater. (1999), https://doi.org/10.1016/S0925-9635(99)00155-7.
[10] L.W. Yin, Y. Bando, M. Sen Li, Y.X. Liu, Y.X. Qi, Unique single-crystalline beta carbon nitride nanorods, Adv. Mater. (2003), https://doi.org/10.1002/adma.200305307.
[11] E. Kovačević, J. Berndt, I. Stefanović, H.-W. Becker, C. Godde, T. Strunskus, J. Winter, L. Boufendi, Formation and material analysis of plasma polymerized carbon nitride nanoparticles, J. Appl. Phys. 105 (2009) 104910, https://doi.org/10.1063/1.3129318.
[12] N.M. Santhosh, G. Filipič, E. Tatarova, O. Baranov, H. Kondo, M. Sekine, M. Hori, K. Ostrikov, U. Cvelbar, Oriented carbon nanostructures by plasma processing: recent advances and future challenges, Micromachines 9 (2018) 565, https://doi.org/10.3390/mi9110565.
[13] M. Meyyappan, L. Delzeit, A. Cassell, D. Hash, Carbon nanotube growth by PECVD: a review, Plasma Sources Sci. Technol. 12 (2003) 205–216, https://doi.org/10.1088/0963-0252/12/2/312.
[14] S. Hussain, E. Kovacevic, J. Berndt, N.M. Santhosh, C. Pattyn, A. Dias, T. Strunskus, M.-R. Ammar, A. Jagodar, M. Gaillard, C. Boulmer-Leborgne, U. Cvelbar, Low-temperature low-power PECVD synthesis of vertically aligned graphene, Nanotechnology 31 (2020) 395604, https://doi.org/10.1088/1361-6528/ab9b4a.
[15] N.M. Santhosh, G. Filipič, E. Kovacevic, A. Jagodar, J. Berndt, T. Strunskus, H. Kondo, M. Hori, E. Tatarova, U. Cvelbar, N-graphene nanowalls via plasma nitrogen incorporation and substitution: the experimental evidence, Nano-Micro Lett. 12 (2020) 53, https://doi.org/10.1007/s40820-020-0395-5.
[16] W. Dawei, F. Dejun, G. Huaixi, Z. Zhihong, M. Xianquan, F. Xiangjun, Structure and characteristics of thin films prepared by rf plasma-enhanced chemical vapor deposition, Phys. Rev. B Condens. Matter 56 (1997) 4949–4954, https://doi.org/10.1103/PhysRevB.56.4949.
[17] X.C. Wang, Z.Q. Li, P. Wu, E.Y. Jiang, H.L. Bai, Annealing effects on the microstructure of amorphous carbon nitride films, Appl. Surf. Sci. (2006), https://doi.org/10.1016/j.apsusc.2006.04.003.
[18] N. Hellgren, N. Lin, E. Broitman, V. Serin, S.E. Grillo, R. Twesten, I. Petrov, C. Colliex, L. Hultman, J.E. Sundgren, Thermal stability of carbon nitride thin films, J. Mater. Res. (2001), https://doi.org/10.1557/JMR.2001.0440.
[19] G.Q. Yu, S.H. Lee, J.J. Lee, Effects of thermal annealing on amorphous carbon nitride films by r, f. PECVD, Diam. Relat. Mater. (2002), https://doi.org/10.1016/S0925-9635(02)00111-5.
[20] Y. Aoi, K. Ono, K. Sakurada, E. Kamijo, M. Sasaki, K. Sakayama, Effects of heat treatment on structure of amorphous CNx thin films by pulsed laser deposition, Thin Solid Films (2001), https://doi.org/10.1016/S0040-6090(01)00888-4.
[21] N. Mutsukura, Photoluminescence and infra-red absorption of annealed a-CNx:H films, Diam. Relat. Mater. (2001), https://doi.org/10.1016/S0925-9635(00)00595-1.
[22] Z. Wang, C. Wang, Q. Wang, J. Zhang, Annealing effect on the microstructure modification and tribological properties of amorphous carbon nitride films, J. Appl. Phys. (2008), https://doi.org/10.1063/1.2978222.
[23] M. Lejeune, O. Durand-Drouhin, S. Charvet, A. Zeinert, M. Benlahsen, On the induced microstructure changes of the amorphous carbon nitride films during annealing, J. Appl. Phys. (2007), https://doi.org/10.1063/1.2747218.
[24] Z.H. Huang, B. Yang, C.S. Liu, L.P. Guo, X.J. Fan, D.J. Fu, Effect of annealing on the composition, structure and mechanical properties of carbon nitride films deposited by middle-frequency magnetron sputtering, Mater. Lett. (2007), https://doi.org/10.1016/j.matlet.2006.11.127.
[25] L. Boufendi, J. Gaudin, S. Huet, G. Viera, M. Dudemaine, Detection of particles of less than 5 nm in diameter formed in an argon-silane capacitively coupled radio-frequency discharge, Appl. Phys. Lett. (2001), https://doi.org/10.1063/1.1425431.
[26] J. Berndt, H. Acid, E. Kovacevic, C. Cachoncinlle, T. Strunskus, L. Boufendi, Deposition and tuning of nanostructured hydrocarbon deposits: from superhydrophobic to superhydrophilic and back, J. Appl. Phys. (2013), https://doi.org/10.1063/1.4789949.
[27] C. Godde, J. Berndt, E. Kovacevic, I. Stefanovic, J. Winter, L. Boufendi, Controlled sampling of nanoparticles in reactive plasmas, IEEE Trans. Plasma Sci. 39 (2011) 2766–2767, https://doi.org/10.1109/TPS.2011.2157980.
[28] A. Bouchoule, A. Plain, L. Boufendi, J.P. Blondeau, C. Laure, Particle generation and behavior in a silane-argon low-pressure discharge under continuous or pulsed radio-frequency excitation, J. Appl. Phys. (1991), https://doi.org/10.1063/1.349484.
[29] E. Kovačević, I. Stefanović, J. Berndt, Y.J. Pendleton, J. Winter, A candidate analog for carbonaceous interstellar dust: formation by reactive plasma polymerization, Astrophys. J. (2005), https://doi.org/10.1086/428392.
[30] P.L. Girard-Lauriault, P. Desjardins, W.E.S. Unger, A. Lippitz, M.R. Wertheimer, Chemical characterisation of nitrogen-rich plasma-polymer films deposited in dielectric barrier discharges at atmospheric pressure, Plasma Process. Polym. (2008), https://doi.org/10.1002/ppap.200800054.
[31] F. Truica-Marasescu, P.L. Girard-Lauriault, A. Lippitz, W.E.S. Unger, M.R. Wertheimer, Nitrogen-rich plasma polymers: comparison of films deposited in atmospheric- and low-pressure plasmas, Thin Solid Films (2008), https://doi.org/10.1016/j.tsf.2008.02.033.
[32] E. Yegen, A. Lippitz, D. Treu, W.E.S. Unger, Derivatization of amino groups by pentafluorobenzaldehyde (PFB) as observed by XPS and NEXAFS spectroscopy on spin coated 4,4′-methylenebis(2,6- diethylaniline) films, in: Surf. Interface Anal., 2008, https://doi.org/10.1002/sia.2685.
[33] P.L. Girard-Lauriault, F. Mwale, M. Iordanova, C. Demers, P. Desjardins, M.R. Wertheimer, Atmospheric pressure deposition of micropatterned nitrogen-rich plasma-polymer films for tissue engineering, Plasma Process. Polym. (2005), https://doi.org/10.1002/ppap.200400092.
[34] N.A. Bullett, D.P. Bullett, F.E. Truica-Marasescu, S. Lerouge, F. Mwale, M.R. Wertheimer, Polymer surface micropatterning by plasma and VUV-photochemical modification for controlled cell culture, Appl. Surf. Sci. (2004), https://doi.org/10.1016/j.apsusc.2004.02.058.
[35] A.V. Syugaev, A.N. Maratkanova, A.A. Shakov, N.V. Lyalina, D.A. Smirnov, Polyaniline films electrodeposited on iron from oxalic acid solution: spectroscopic analysis of chemical structure, J. Solid State Electrochem. (2018), https://doi.org/10.1007/s10008-018-4033-9.
[36] A.G. Shard, J.D. Whittle, A.J. Beck, P.N. Brookes, N.A. Bullett, R.A. Talib,

A. Mistry, D. Barton, S.L. McArthur, A NEXAFS examination of unsaturation in plasma polymers of allylamine and propylamine, J. Phys. Chem. B (2004), https://doi.org/10.1021/jp048250f.
[37] C. Pattyn, E. Kovacevic, T. Strunskus, T. Lecas, J. Berndt, Formation and behavior of negative ions in low pressure aniline-containing RF plasmas, Sci. Rep. (2019), https://doi.org/10.1038/s41598-019-47425-9.
[38] J. Stöhr, NEXAFS Spectroscopy, Springer Berlin Heidelberg, Berlin, Heidelberg, 1992, https://doi.org/10.1007/978-3-662-02853-7.
[39] F. Alvarez, M.C. dos Santos, Electronic and structural properties of amorphous carbon–nitrogen alloys, J. Non-Cryst. Solids 266–269 (2000) 808–814, https://doi.org/10.1016/S0022-3093(99)00820-0.
[40] U. Oran, S. Swaraj, A. Lippitz, W.E.S. Unger, Surface analysis of plasma deposited polymer films, 7: "In situ" characterization of plasma deposited allylamine films by ToF-SSIMS, XPS and NEXAFS spectroscopy, Plasma Process. Polym. (2006), https://doi.org/10.1002/ppap.200500168.
[41] S. Bhattacharyya, M. Lübbe, P.R. Bressler, D.R.T. Zahn, F. Richter, Structure of nitrogenated amorphous carbon films from NEXAFS, Diam. Relat. Mater. (2002), https://doi.org/10.1016/S0925-9635(01)00525-8.
[42] H. Yabuta, M. Uesugi, H. Naraoka, M. Ito, A.L.D. Kilcoyne, S.A. Sandford, F. Kitajima, H. Mita, Y. Takano, T. Yada, Y. Karouji, Y. Ishibashi, T. Okada, M. Abe, X-ray absorption near edge structure spectroscopic study of Hayabusa category 3 carbonaceous particles, Earth Planets Space (2014), https://doi.org/10.1186/s40623-014-0156-0.
[43] L. He, F. Weniger, H. Neumann, M. Beller, Synthesis, characterization, and application of metal nanoparticles supported on nitrogen-doped carbon: catalysis beyond electrochemistry, Angew. Chem. Int. Ed. (2016), https://doi.org/10.1002/anie.201603198.
[44] R. Arrigo, M.E. Schuster, Z. Xie, Y. Yi, G. Wowsnick, L.L. Sun, K.E. Hermann, M. Friedrich, P. Kast, M. Hävecker, A. Knop-Gericke, R. Schlögl, Nature of the N-Pd interaction in nitrogen-doped carbon nanotube catalysts, ACS Catal. (2015), https://doi.org/10.1021/acscatal.5b00094.
[45] I. Jiménez, R. Gago, J.M. Albella, L.J. Terminello, X-ray absorption studies of bonding environments in graphitic carbon nitride, Diam. Relat. Mater. (2001), https://doi.org/10.1016/S0925-9635(00)00383-6.
[46] R. McCann, S.S. Roy, P. Papakonstantinou, M.F. Bain, H.S. Gamble, J.A. McLaughlin, Chemical bonding modifications of tetrahedral amorphous carbon and nitrogenated tetrahedral amorphous carbon films induced by rapid thermal annealing, in: Thin Solid Films, 2005, https://doi.org/10.1016/j.tsf.2004.11.151.
[47] S. Pellegrino, L. Beck, P. Trouslard, Differential cross-sections for nuclear reactions 14N(d,p5)15N, 14N(d,p0)15N, 14N(d,α0)12C and 14N(d,α1)12C, Nucl. Instrum. Methods Phys. Res. Sect. B Beam Interact. Mater. Atoms 219–220 (2004) 140–144, https://doi.org/10.1016/j.nimb.2004.01.042.
[48] W.N. Lennard, G.R. Massoumi, P.F.A. Alkemade, I.V. Mitchell, S.Y. Tong, Revisiting the 12C(d,p)13C reaction cross section using condensed gas targets, Nucl. Instrum. Methods Phys. Res. B (1991), https://doi.org/10.1016/0168-583X(91)95552-O.
[49] P. Plantin, A.-L. Thomann, P. Brault, B. Dumax, J. Mathias, T. Sauvage, A. Pineau, Study of deposition and post-oxidation of d.c. magnetron sputtered W/Fe bilayers, Surf. Coating. Technol. 200 (2005) 408–412, https://doi.org/10.1016/j.surfcoat.2005.01.055.
[50] S.S. Roy, P. Papakonstantinou, T.I.T. Okpalugo, H. Murphy, Temperature dependent evolution of the local electronic structure of atmospheric plasma treated carbon nanotubes: near edge x-ray absorption fine structure study, J. Appl. Phys. (2006), https://doi.org/10.1063/1.2260821.